p62 promotes HIV-1 gp120 V3 loop-mediated microglial inflammation by promoting noncanonical activation of Nrf2

Sisi Liu
Jinan University
Xueqin Yan
Jinan University
Hanyang He
Jinan University
Rui Pan
Jinan University
Haijie Tang
Jinan University
Huili Wang
Jinan University
Saixian Wen
Jinan University
Limeng Gan
Jinan University
Guangming Li
Jinan University
Yongmei Fu
Jinan University
Jun Dong (dongjunbox@163.com)
Department of Pathophysiology,Laboratory of Pathophysiology,State Administration of Traditional Chinese Medicine,School of Medicine,GHM Institute of CNS Regeneration,Jinan University,Guangzhou
https://orcid.org/0000-0002-6064-0814

Research Article

Keywords: HIV-1- associated neurocognitive disorders, HIV-1 gp120 V3 loop, Autophagy, p62, Nrf2, HO-1

Posted Date: February 23rd, 2021

DOI: https://doi.org/10.21203/rs.3.rs-222430/v1

Abstract

Combined antiretroviral therapy (cART) has significantly increased the life expectancy of AIDS patients; however, the prevalence of the neurocognitive impairment associated with HIV-1 continues to rise. HIV-1 gp120, an important subunit of the envelope spikes that decorate the surface of virions, is found to activate microglia in central nervous system (CNS) which leads to the cognitive and behavioral dysfunction known as HIV-1 associated neurocognitive disorder(HAND), and the V3 loop is the most important toxic domain of gp120. A study has shown that autophagy plays key role in the activation of microglia, p62 is an important autophagy substrate protein that is elevated in neuroinflammation. In this study, we sought to explore the role of p62 in gp120 V3 loop-mediated microglial activation. Our results demonstrated that exposure of CHME-5 cells to the gp120 V3 loop resulted in elevated inflammatory cytokines, accompanied by autophagy dysfunction and p62 upregulation. Subsequently, we found that the p62-dependent Nrf2 noncanonical signaling pathway was activated and that HO-1, the target protein of Nrf2, was also upregulated. Interestingly, the elevation of inflammatory factors caused by the gp120 V3 loop was significantly alleviated after knocking down p62, Nrf2 and HO-1. Further investigation revealed that in the microglial inflammation induced by the gp120 V3 loop, up-regulated HO-1 promoted the expression of iNOS by interacting with iNOS, while enhanced autophagy by RAPA promoted the degradation of iNOS and alleviated inflammation. These findings provide a new perspective on the relationship between noncanonical Nrf2 activation and autophagy in microglial inflammation and an experimental basis for HAND prevention and treatment.

Introduction

HIV-1 not only destroys the peripheral immune system, but also infringes on the central nervous system and causes cognitive, motor or behavioral abnormalities[1,2], known as HIV-1 associated neurocognitive disorder (HAND)[3] . Dispite the extensive application of cART, the prevalence rate of HAND is still rising, due to the poor biological permeability and toxicity of drugs[4,5]. Therefore, it is urgent to explore and clarify the pathogenesis of HAND to provide a basis for its prevention and treatment. The main pathogenesis of HAND is the activation of microglial cells by HIV-1 associated proteins, such as gp120, and the release of proinflammatory cytokines, which results in the neuronal injury[6,7]. Our previous studies have shown that the gp120 peptide can promote autophagy in BV2 microglia[8], but the specific mechanism of autophagy regulation in microglia is still unclear.

Macroautophagy, hereafter referred to as autophagy, is an important mechanism by which cells to maintain their homeostasis. Autophagy begins with the formation of phagocytic vesicles, and then the membrane of phagocytic vesicles stretches to form autophagosomes with a unique double-membrane structure. The whole autophagosome then fuses with the lysosome to form an autolysosome, containing a series of lysosomal degrading enzymes (such as cathepsin and other acidic hydrolases) that digested the tomont contents of the autolysome. In this study, we selected three autophagy-associated proteins such as LC3, Beclin-1 and p62, as indicators and assessed autophagic flux to determine the autophagy level and function. Autophagy flux is currently the most reliable method for measuring autophagy, which

uses labeling of LC3 with vectors (such as plasmid, adenovirus, lentivirus, etc.) in tandem with GFP(green fluorescent protein)and RFP(red fluorescent protein) to reflect the process of autophagy.

p62 is an important autophagy adaptor protein that can recruit ubiquitinized substrates to autophagosomes for degradation and is eventually degraded in autolysosomes[9]. Therefore, the cellular level of p62 has been considered a marker for autophagy activity, and the amount of p62 is considered to be inversely correlated with autophagic flux[10]. It is also worth noting that p62 is also a multifunctional signaling center that is involved in a variety of cellular activities such as apoptosis, inflammation, and the oxidative stress response[9]. p62 directly binds to Keap-1 and thus leads to the noncanonical activation of Nrf2. In general, Nrf2 is stored in the cytoplasm in an inactive state and is mainly negatively regulated by Keap-1, which can induce cullin3 E3 ubiquitin ligase to promote the ubiquitination of Nrf2 and its degradation by the proteasome. Haefen et al found that in an LPS-induced model of central nervous inflammation in rats, toxic lentils can reduce neuroinflammation by reducing p62 levels and improving autophagy dysfunction[11]. Additionally, Jin et al reported that koumine can reduce the level of p62 and further inhibit the activation of astrocytes[12]. Moreover, it has been reported that in a rat model of stress hypertension, glial cells are largely activated and release inflammatory cytokines such as IL-1β and TNF-α , while minocycline can alleviate inflammation by reducing p62 levels[13]. These studies have shown that the high-expression of p62 is common in a neuroinflammation model, but the exact pathogenesis is not clear, nor is its role in HAND.

Nrf2 is a transcription factor belonging to cap 'n' collar family of zippers, and there are two ways to activate Nrf2 that are known. Under oxidative stress, the canonical activation of ROS and other electrophiles modifies the specific cysteine of Keap1, thereby blocking the ubiquitination degradation pathway of Nrf2, and increasing the level of Nrf2 further promotes its downstream protein expression[14]. The other way is the noncanonical way, in which various reasons cause autophagy dysfunction leading to p62 accumulation, after which p62 binds to Keap-1 competitively so that the level of Nrf2 increases[15], while p62 is also one of the target protein of Nrf2, with the p62-dependent upregulation of NRF2 increasing the transcription of p62 itself, creating a positive feedback loop that promotes the prolonged activity of NRF2, leading to intracellular redox imbalance[16,17]. Based on these data outlined above, this study investigated the role and mechanism of p62 mediating crosstalk between autophagy and the Nrf2 noncanonical signaling pathway in HIV-1 gp120 V3 loop-mediated microglial inflammation.

Result

HIV-1 gp120 V3 loop-mediated defective autophagy increases microglial activation and elevates proinflammatory cytokines in CHME-5 cells

First, we observed the level of inflammatory cytokines released by microglia induced by thebHIV-1 gp120 V3 loop. TNF-α, MCP-1 and IL-1β were chosen as markers of inflammation. As seen in figure 1A, the gp120 V3 loop can induced the upregulation of these inflammatory factors, while the autophagy inducer rapamycin can inhibited this effect.

Based on the changes in inflammatory cytokines, we then observed the effect of the HIV-1 gp120V3 loop on autophagy in CHME-5 cells. Since autophagy is a dynamic process, we used the GFP-RFP-LC3 adenovirus to infect cells to study the changes in autophagic flux in CHME-5 cells treated with or without HIV-1 gp120 V3 loop. Following the formation of the autophagosomes, LC3 is labeled with both red and green fluorescence that appeared as merged yellow puncta due to the colocalization of GFP and RFP-LC3B. However, under a pH<4 condition, the GFP signal of the adenovirus-expressed fluorescently tagged LC3B fusion protein is quenched, whereas the red fluorescence remains stable, showing red after the overlay. The increased accumulation of the yellow puncta is thus an indicator of impaired autophagy, while the increased accumulation of the red puncta indicates increased autophagic flux (figure 1B). As shown in figure 1(B, C), CHME-5 cells transfected with the GFP-RFP-LC3 adenovirus followed by exposure to the HIV-1 gp120 V3 loop (50 ng/mL) for 24 h, exhibited a significant increase in the yellow puncta compared with the random peptide group (the control group), with significantly more yellow puncta than red puncta in the group, indicating incomplete autophagosome maturation. However, decreased numbers of yellow puncta were observed in CHME-5 cells exposed to rapamycin (20 nM), an autophagy flux inducer, along with an increased formation of red puncta (figure 1B, C)), indicating increased autophagy flux. Next, we assessed changes in the levels of the autophagy-related proteins Beclin-1, LC3 and p62. As shown in figure 1C, western blot analysis indicated that the gp120 V3 loop increased the expression of LC3, Beclin-1 and p62, while pretreatment with RAPA reversed these effects in CHME-5 cells(figure 1D). Therefore, these results indicate that the gp120 V3 loop can increase proinflammatory cytokines and mediate autophagy dysfunction in CHME-5 cells, while promoting autophagy with RAPA can improve microglial inflammation caused by the gp120 V3 loop

Silencing of p62 or Nrf2 can prevent HIV-1 gp120 V3 loop mediated increased proinflammatory cytokines in CHME-5 cells

Next, we wanted to explore whether silencing the autophagy-associated protein p62 or its related signaling molecule Nrf2 genes could alleviate inflammation in CHME-5 cells treated with the gp120 V3 loop. Therefore, inflammatory cytokines such as TNF-α, MCP-1 and IL-1β were assessed in gp120 V3 loop-exposed CHME-5 cells transfected with either p62 siRNA or Nrf2 siRNA (figure 2A, C). As shown in figure 2B and D, silencing of both p62 and Nrf2 reversed the upregulation of inflammatory cytokines induced by the gp120 V3 loop in CHME-5 cells. These results suggest that silencing of p62 and Nrf2 can prevent HIV-1 gp120 V3 loop-mediated increases in proinflammatory cytokines in CHME-5 cells.

HIV-1 gp120 V3 loop leads to noncanonical activation of Nrf2 in CHME-5 cells

To further study the mechanism by which silencing p62 or Nrf2 can prevent HIV-1 gp120 V3 loop-mediated increases in proinflammatory cytokines in CHME-5 cells, we observed the exact activation way of Nrf2 in CHME-5 cells treated with the gp120 V3 loop. As mentioned above, Nrf2 can be activated in two ways, among which noncanonical activation is marked by the competitive binding of p62 to Keap-1, which is the negative regulator of Nrf2. First, we observed the effect of the knockdown of p62 on Nrf2 signaling pathway-related protein levels, including Nrf2 cytoplasmic and nuclear levels, Keap-1, and the

Nrf2 target protein HO-1 (figure 3 A, B). The results show that in the gp120 V3 loop treatment group, Nrf2 was increased in both the cytoplasm and the nucleus, as well as Keap-1 and HO-1and that knockdown p62 could reverse these changes caused by the gp120 V3 loop. Moreover, immunoprecipitation assays revealed an interaction between p62 and Keap-1 in CHME-5 cells treated with the gp120 V3 loop (figure 3C), which is a prominent sign of noncanonical activation of Nrf2. To further explore the relationship between p62 and Keap-Nrf2 signaling, we observed changes in p62 and Keap-1 protein levels after silencing Nrf2. Figure 3D shows that silenting Nrf2 significantly reduced the levels of p62 and Keap-1, which indicates that p62 and Keap-1 are also targets of Nrf2 in CHME-5 cells treated with the gp120 V3 loop. In summary, these results suggest that the gp120V3 loop induces Nrf2 noncanonical activation of in CHME-5 cells.

HO-1 promotes iNOS expression by interacting with iNOS to promote inflammation in HIV-1 gp120 V3 loop treated CHME-5 cells.

We next explored the mechanism of inflammation in CHME-5 cells induced by noncanonical activation of Nrf2 induced by the gp120 V3 loop. In a previous study, we found that HO-1, the target protein of Nrf2, was increased in the gp120 V3 loop treatment group. Therefore, we performed a knockdown of HO-1 with RNA interference (figure 4A), and we found that the TNF-α, MCP-1 and IL-1β levels were significantly decreased compared with the gp120 V3 loop group after knockdown of HO-1(figure 4C). At the same time, we found that the knockeddown of HO-1 can significantly reduced the protein level of iNOS(figure 4B), Immunofluorescence staining results showed that iNOS and HO-1 levels in the gp120 V3 loop group were upregulated and colocalized (figure 4D) ; however, iNOS protein levels were significantly decreased in the HO-1 knockdown group compared to the gp120 V3 loop group. These results suggest that the HIV-1 gp120 V3 loop can up-regulate HO-1, which interacts with iNOS to promote inflammation.

Rapamycin promotes the degradation of iNOS through autophagy in HIV-1 gp120 V3 loop treated CHME-5 cells

To explore whether the upregulation of iNOS was related to impaired autophagy in addition to its interaction with HO-1, we used the autophagy inducer rapamycin to observe the relationship between autophagy and iNOS levels in HIV-1 gp120 V3 loop treated CHME-5 cells. As seen in figure 5, compared with the gp120 V3 loop group, the autophagy inducer rapamycin plus gp120 V3 loop group showed significantly decreased iNOS levels in both the immunofluorescence assay (figure 5A) and the western blot (figure 5B, C). In addition, we further found by an immunofluorescence assa that the autophagy inducer rapamycin could downregulate the expression of iNOS. These results suggest that rapamycin promotes the degradation of iNOS through autophagy in HIV-1 gp120 V3 loop-treated CHME-5 cells.

Brusatol alleviates neurocognitive dysfunction in mice induced by the HIV-1 gp120 V3 loop

Because our in vitro data suggested that silencing Nrf2 can reduce inflammation caused by the gp120 V3 loop, we used brusatol, an inhibitor of Nrf2, to verify the mechanism by which noncanonical activation of Nrf2 promotes microglial inflammation in vivo. We first observed the alleviation effect of brusatol on

learning and memory dysfunction induced by the gp120 V3 loop in mice. The Water maze and Step-through passive avoidance test were used to evaluate learning and memory function in our research. Mice were randomly divided into four groups, and the details of the groups were the same as those described previously (Materials and Methods). As seen in figure 6A and B, the gp120V3 loop prolonged escape latency significantly, while brusatol reversed the effects on the 5^{th} and 6^{th} days of testing. Representative search strategy trials also showed a difference between the gp120 V3 loop group and the gp120 V3 loop plus brusatol group (figure 6A). Similarly, in the probe trial, the group injected with the gp120V3 loop demonstrated fewer platform crosses and spent less time in the target quadrant than that of the random peptide group, while the group administered with the gp120V3 loop and brusatol demonstrated more platform crosses and spent more time in the target quadrant than did the group administered with the gp120V3 loop alone. The representative search strategy trials in the probe test were also showed that mice in the gp120 V3 loop plus brusatol group performed better in finding the platform than those in the gp120 group (figure 6B). Furthermore, the results of the Step-through passive avoidance test showed that the brusatol group showed longer latency and fewer errors than the gp120V3 loop group (figure 6C and 6D). These data suggested that brusatol alleviates cognitive impairments caused by the HIV-1gp120 V3 loop.

Brusatol inhibits HIV-1 gp120 V3 loop mediated increased autophagy marker expression, microglial activation and proinflammatory cytokines in mice

To further confirm the the role of Nrf2 in microglial inflammation induced by the gp120 V3 loop, Western blotting was used to observe the levels of autophagy-related proteins, Nrf2 signaling related proteins and iNOS levels in the brain tissues of mice in each group. As shown in figure 7 A and 7 B, we found that compared with the control group, Beclin-1, LC3 and p62 in the gp120 group were significantly upregulated, suggesting autophagy dysfunction, that Nrf2, Keap-1 and HO-1 were upregulated, indicating that Nrf2 was noncanonical activated; and that iNOS significantly upregulated inflammation. However, brusatol can further promoted the upregulation of Beclin-1 and LC3, and downregulated p62, indicating that brusatol alleviated autophagy dysfunction caused by the gp120 V3 loop, and downregulated Nrf2, Keap-1, HO-1 and iNOS, indicating that brusatol can inhibited the noncanonical activation of Nrf2. Furthermore, the ELISA results showed that the gp120 V3 loop promoted the upregulation of inflammatory factors in brain tissues (including TNF-α, MCP-1 and IL-1β), while brusatol alleviated inflammation (figure 7C). To further confirm the role of autophagy in microglial activation, we next performed immunofluorescence staining for autophagy-associated protein p62 and microglial marker Iba-1 in the hippocampus (figure 8A) and the cortex (figure 8B) of the mice from each group. As shown in figure 8, the intensity of the p62 (green) and Iba-1 (yellow) puncta formation was significantly increased in the hippocampus and cortex of gp120V3 loop mice compared to the random peptide group. Furthermore, the red fluorescence (Iba-1) was significantly increased and colocalized with the autophagy-associated protein p62 (green) in the gp120 V3 loop group. These findings thus underscore the effects of brusatol on HIV-1 gp120 V3 loop-mediated increased autophagy marker expression, microglial activation and proinflammatory cytokines in mice.

Discussion

Studies have shown that neuroinflammation of caused by HIV-1 activated microglia is the key factor in the occurrence and development of HAND [18,19]. Microglia are the most important immune cells in the brain tissue and are widely distributed in the brain[20]. There is also evidences showning that even in HAND patients treated with HAART(highly active antiretroviral therapy), the severity of the disease is related to the activation of microglia cells[19]. gp120, which is an envelope protein of the HIV-1 virus, can can induce a series of inflammatory factors, such as TNF-α, MCP-1, IL-1β, IL-6 and iNOS by binding the corresponding receptors on the microglial cell surface, and these inflammatory factors can act on other glial cells to amplify the neuroinflammation. In this study, the HIV-1 gp120 V3 loop was used, which is the third variable region of gp120[21] and the most important structural domain of gp120-induced toxicity[22]. In addition, random peptide segments were selected as the control, ensuring the scientific nature of the control.

Autophagy is associated with inflammation, tumors, neurodegenerative diseases and other diseases. Recent studies, including our preliminary study, have demonstrated the role of impaired autophagy in neurons as a correlate of neurodegeneration in HAND[23-25]. However, the specific mechanism by which autophagy regulating microglial activation remains unclear. In this study, we demonstrated that the persistent stimulation of the HIV-1 gp120 V3 loop impaired the integration of autophagosomes and lysosomes in CHME-5 cells. Additionally, inflammatory factors were increased in CHME-5 cells treated with the gp120 V3 loop and reduced when treated with rapamycin simultaneously, suggesting that autophagy dysfunction promotes inflammation.

We further observed the changes in autophagy-related proteins and found that p62 was upregulated. Intracellular proteins or organelles can be degraded by two pathways: the proteasome pathway and the autophagy lysosome pathway. p62, as an autophagy substrates of chitosan protein combines with LC3 through polymerization , and is degraded in the targeted autophagosome [26], which is the main negative regulatory mechanism by which p62 maintain its basic level in cells, an thus it is possible that autophagy dysfunction causes abnormal accumulation of p62. Furthermore, abnormal accumulation of p62 affects many signaling pathways due to its special structure, and studies have shown that a lack of p62 in mice results in lower energy consumption and fever, as well as lower transcription [27]. This may be related to p62 participating in nutritional mTORC1 activation in sensing to adjust the adipocyte differentiation and energy controlling[27,28]. Interestingly, inflammatory factors were reduced after p62 knockdown in our in vitro studies, suggesting that p62 accumulation may promote microglial inflammation, which is consistent with the results of many studies. For example, excessive accumulation of p62 causes the inflammatory environment to promote the occurrence of hepatocellular carcinoma[29], and there is a large amount of p62 accumulation in microglial toxic reactions caused by trimethyl tin chloride[30]. The canonical activation of Nrf2 is caused by the conformational changes in Keap-1 caused by various oxidative stimuli, and the dissociation of Keap-1 and Nrf2 causes the activation of Nrf2, in which p62 is not involved. p62 is involved in the noncanonical activation of Nrf2, which is characterized by the competitive binding of p62 to Keap-1, the main negative regulator of Nrf2[15]. After Nrf2 activation

and incorporation into the nucleus, the antioxidant damage effects of target genes such as HO-1, NQO1 and GSH have been confirmed, and it cannot be ignored that some studies have noticed the negative effects of Nrf2, such as liver fibrosis, liver injury and Kaposi's sarcoma as mentioned above. In nervous system diseases, neurofibrillary tangling of brain tissue of AD brain tissue was found to polymerize the phosphorylated p62-Keap-1 complex, and the expression of the Nrf2 target gene was increased simultaneously[31-33]. However, the relationship between the noncanonical activation of Nrf2 and HAND was still unknown. In this study, we found that autophagy dysfunction in CHME-5 cells caused by HIV-1 gp120 V3 loop led to the upregulation of p62 and the release of inflammatory factors. In addition, Keap-1 expression was up-regulated, and the knockdown of p62 could reduce Nrf2 levels. Combined with the Co-IP results, this indicated that Nrf2 was noncanonically activated by p62. Furthermore, inflammatory factors were downregulated after the knockdown of Nrf2, suggesting that noncanonically activated Nrf2 was related to inflammation.Nrf2 was related to inflammation. In addition, Keap-1 and p62 have also found to be the target proteins of Nrf2[34,35]. This indicates that when Nrf2 is activated, Keap-1 and p62 levels are upregulated, and thus p62-Nrf2 forms a positive feedback loop, which was also confirmed in our study, which also showed that inflammatory cytokines were downregulated after blocking this positive feedback in gp120 V3 loop-treated CHME-5 cells. Therefore, the continuous upregulation of p62, Keap-1 and Nrf2 levels leads to the imbalance of intracellular redox.

HO-1, one of the target proteins of Nrf2, was found to be correlated with inflammation or oxidative stress in lung ischemia reperfusion[36]. In our study, HO-1 and iNOS were both upregulated and co-localized, as observed by immunofluorescence detection. Interestingly, iNOS was downregulated after knocking down HO-1, it is suggesting that HO-1 can promote iNOS expression by interacting with it, but the specific sites of its interaction need to be further studied.

In vivo, a HAND mouse model was constructed by 8-week-old SPF mice injected with the HIV-1 gp120 V3 loop in the lateral ventricle. This model is copied based on the papers previously published by our research group[37] , but it is less difficult and more reproducible than the previous rat model. In the pre-experiment, the brain was harvested for observation 10 min after the injection of trypan blue for 10 min, so as to ensure the accuracy of the injection mode and the injection point. Brusatol is a specific blocker of Nrf2 that can rapidly reduce the expression of Nrf2 independent of on Keap-1. It has been reported that brusatol may reduce the protein level of Nrf2 through demethylation[38] and has a strong lipid solubility to allow it to cross the blood-brain barrier. Brusatol can inhibit cytokine dependent induction of iNOS[39] in β cells, furthermore, brusatol can inhibit the c-myc /ROS signaling pathway in rectal cancer[40]. Our study found that brusatol alone had no significant effect on behavior or inflammatory factor expression in mice, while it can significantly improved the performance of the water maze and step-through passive avoidance in mice lateral in the lateral ventricle with gp120 V3 loop. Further experiments showed that brusatol reduced the release of inflammatory cytokines in mouse brain tissue induced by the HIV-1 gp120 V3 loop and reduced the expression of the mouse hippocampus and cortex microglia marker protein Iba-1. Molecular biology experiments found that Nrf2, Keap-1, HO-1 and iNOS expression was upregulated in the gp120 V3 loop group, autophagy-related proteins Belin-1, LC3 and p62 was upregulated, and the microglial marker protein iba-1 was upregulated and colocalized with p62 and LC3. Brusatol inhibited the

noncanonical activation of p62-dependent Nrf2 induced by the gp120 V3 loop, and the downregulation of p62 and Keap-1 suggested that inhibition of Nrf2 blocked the positive feedback loop of p62-Nrf2. Therefore, the results of the in vitro experiments were verified well by the reduction in the level of inflammatory cytokines in the brain tissue and in reducing the impairment of learning and memory function in mice.

Conclusions

This study investigated the role of p62 in CHME-5 cells inflammation induced by the HIV-1 gp120 V3 loop. We demonstrated that the gp120 V3 loop can cause autophagic flow blockade, cause p62 accumulation, promote noncanonical activation of Nrf2, upregulate the level of HO-1, interact with iNOS to upregulate inflammation, and degrade iNOS through the autophagic lysosome pathway. Thus, targeting the noncanonical activation of Nrf2 in microglia may provide a novel therapeutic approach to treat HAND.

Materials And Methods

Cell Culture and Treatment

CHME-5 cells were cultured in a 25-cm^2 culture flask with High Glucose DMEM (Gibco/Thermo-Fisher, Waltham, MA, USA) supplemented with 5% fetal bovine serum (Hyclone/GE, Logan, UT). at 37 °C in a humidified atmosphere containing 5% CO_2. cells were pretreated with 20 nM rapamycin (Sigma, USA) for 1 h and then co-treated with HIV-1 gp120V3loop (Shanghai, China;
sequence: NNTRKSIRIQRGPGRAFVTIGKIG; molecular formula:$C_{114}H_{199}N_{41}O_{31}$;molecular weight: 2640.06, 1 μg/mL) another 24 h, the RP group were pretreated with random peptide (Shanghai, China; sequence: KCSEYKKWIDLKKSEYKVDKYKK; molecular weight: 3066.64 kD, 1 μg/mL)

Western Blot Analysis

The cells were treated according to the study design and harvested, The brain samples were suspended in buffer solution and then centrifuged at 12,000 rpm for 30 min at 4°C. The supernatant was separated and collected for protein analysis. Protein was extracted using a protein extraction kit (Beyotime, China), and the concentration was determined using a Bio-Rad Protein Assay. The cytosolic and nuclear fractions were separated using a nuclear and cytoplasmic protein extraction kit, according to the manufacturer's instructions (WLA020a, Wanleibio Co., Ltd. Shenyang China). SDS–polyacrylamide gels were used for separation via electrophoresis and then transferred to polyvinylidene fluoride membranes at 120 V for 30 min and 80 V for 2 h. The transferred membranes were blocked using fresh 5% nonfat dry milk dissolved in Tris-buffered saline Tween-20 (TBST) at room temperature for 1 h. The immunoblots were then probed with the appropriate antibodies. Primary antibodies used were: anti-GAPDH (5174s), anti-p62 (23214s), beclin-1 (3495s), anti-LC3 (3868s) anti-Keap1 (4678s) were purchased from Cell Signaling Technology, and anti-Nrf2 (WL02135, 1:1000, Wanleibio, Shenyang, China), anti-Lamin B (WL01775,1:1000, Wanleibio,

Shenyang, China), anti-HO-1 (ab223349, 1:1000, Abcam), anti-iNOS (ab178945, 1:1000, Abcam). Each primary antibody was individually incubated with the membrane at 4°C for 12 h. Following incubation with primary antibodies and washing three times with TBST for 10 min each, the membranes were incubated for 1 h with the appropriate secondary antibody (diluted 1:5000 in TBST, 5% skim milk) and subsequently washed an additional three times with TBST for 10 min each. The detection of specific proteins was performed with an enhanced chemiluminescent detection system. The bands were quantified by densitometry using Image-ProPlus 6.0.

ELISA

TNF-a, MCP-1 and IL-1β kits (USCN Business Co., Ltd, China) were used to determine the cytokine levels in mouse serum according to the manufacturer's instructions.

RFP-GFP-LC3 Adenovirus Transfection

To analyse autophagic flux, CHME-5 cells were transfected with mRFP-GFP-LC3-expressing adenovirus (Genechem Co.,Ltd. China), according to the manufacturer’s instructions. The procedure was performed as follows: the CHME-5 cells were plated on a confocal dish and treated with 250 μL of infection enhancement medium containing 1×10^5 PFU RFP-GFP-LC3-expressing adenovirus. After 2 h of incubation, the medium was replaced by the adenovirus-free medium. Later, at 24 h, the treatment solutions were then applied to the plate, followed by incubation for 24 h. The images were acquired with an Leica fluorescence microscope with the cells fixed.

SiRNA transfection

CHME-5 cells were transfected either with p62, Nrf2 or HO-1 siRNAs. Briefly, mPMs were seeded into 6-well plate at a density of 3×10^5 cells/well and cultured in a humidified, 5% CO2 incubator at 37°C. On the next day, the culture medium was replaced with Opti-MEM® I Reduced Serum Medium. Meanwhile, the individual targeted siRNA and scrambled siRNA (500 pmol/ml) and Lipofectamine® 2000 (2 μl/ml) were incubated separately with Opti-MEM® I Reduced Serum Medium for 5 min at room temperature. After incubation, both individually targeted siRNAs and Lipofectamine® 2000 mix were mixed and subsequently, incubated at room temperature for another 15 min, mixed liquids were gently added to the culture medium. After 6 to 8 h the culture medium was replaced with DMEM supplemented with 10% heat-inactivated FBS. The transfected mouse primary microglia cells were then exposed to HIV-1 gp120V3 loop for 24 h, and transfection efficiency was analyzed by western blotting. All experiments were repeated at least 6 times.

Co-Immunoprecipitation

CHME-5 cells were lysed and analyzed using previously established protocols in Western Blot Analysis. Lysates were centrifuged at 12,000 g for 15 min at 4 °C. Cleared lysates were incubated overnight with the indicated antibodies and for 1 h with protein A/G beads (Med Chem express, USA). The pellets were then

washed four times with ice-cold lysis buffer. The immunoprecipitation samples were eluted from the beads by heating with SDS sample buffer. Eluted immunoprecipitates or whole cell lysates were separated by SDS-PAGE and analyzed by western blot.

Immunofluorescence Analysis

In vitro: After incubation according to the study design, the CHME-5 cells were fixed with 4% PFA in PBS for 30 min, washed with PBS three times and then permeabilized with Triton-X-100 for 15 min. After washing with PBS three times, the cells were blocked with 5% BSA for 1 h at room temperature and then incubated with anti-HO-1 (ab223349, 1:100, Abcam), anti-iNOS (ab178945, 1:100, Abcam) in 5% BSA overnight at 4 °C. Subsequently, the cells were washed in PBS three times and incubated with fluorescein isothiocyanate-labeled secondary antibody for 1 h at 37 °C. The cells were then washed and incubated with DAPI for 15 min and then washed again and mounted. The cells were then imaged using Leica fluorescence microscope.

In vivo: After irrigation with 4% PFA, the brain tissue was removed and fixed in PFA for 24h. After washing with PBS for three times, 10% sucrose →20% sucrose →30% sucrose was used for gradient dehydration, and then oct-embedded and frozen at -80°C for about 40min before sectioning. The brain was cut into 20 m thick coronal sections with a frozen slicer, and baked for 2h at 38-40°C on a sheet baking machine. After drying to room temperature, the tissue slices could be stained with immunofluorescence. Sections (10 μm thick) were cut and mounted on microscope slides. Staining of p62 and Iba-1 using anti- p62 (1:100, 23214s, Cell Signaling Technology), anti- Iba-1 (1:100, ab5076, Abcam) primary antibodies were performed in mouse hippocampus and cortex.

Animals and intracerebroventricular injection

Male C57BL6J mice (8 weeks old) were procured from Shandong Experimental Animal Center (37009200014313). All animals were kept under a 12-hour light/12-hour dark cycle and allowed free access to water and food. mice were housed in wire cages at 20–22℃ and 50 ± 5% humidity. All experiments were approved by the Laboratory Animal Ethics Committee of Jinan University.

Intracerebroventricular injection: mice were anesthetized with 1.2% tribromoethanol and placed in a stereotaxic apparatus (RWD Life Science, Shenzhen China). A burr hole was drilled 0.2-0.5 mm posterior to bregma and 1.0 mm lateral to the midline, and the lateral ventricle was injected with a micro syringe at 2.5-3.0mm below the skull. The sham group was given random peptides and gp120V3 loop group was given 100ng/5μL/d, which was administered continuously for 3 days, once a day. After lateral ventricle injection, the brusatol group and gp120V3 loop+brusatol group were intraperitoneally injected with 2 mg/kg of brusatol, once every other day, until sampling. The control group and gp120 group were intraperitoneally injected with the same amount of normal saline. The random peptide and gp120 were dissolved with artificial cerebrospinal fluid (ACSF: NaCl 124.0 mM, KCl 3.0 mM, CaCl2 2.0 mM, MgCl2 2.0 mM, NaHCO3 26 mM, NaH2PO4 1.25 mM, Glucose 10.0 mM, pH 7.3-7.4).

Morris water maze

The Morris water maze test is used to assess memory. We performed this test as described by Morris et al [41]. A circular plastic pool (height: 60 cm, diameter: 120 cm) was filled with milk kept at 22–24°C. An escape platform (height: 30 cm, diameter: 10 cm) was submerged 1-1.5 cm below the surface of the water in position. A camera was fixed to the ceiling above the water maze and connected to a computer-based program (Ethovision XT, Noldus Netherlands). mice were tested over 5 days (four trials/day) to find the hidden escape platform in the bottom left quadrant. They had a maximum of 60 s to find the platform. If animals were unable to locate the platform, they were gently guided to the platform and required to stay on the platform for 30 s before being removed. Mice were subjected to a probe trial by removing the platform during 60s. The number of rats crossing the target quadrant and time spent in the target quadrant were used as measures of spatial memory.

Step-Through Passive Avoidance test

Step-Through Passive Avoidance test is a behavioral experiment designed to observe the short-term memory reproduction ability of mice. The experimental device (Chengdu tmin life technology co., LTD) is half dark room and half-light room, connected with adjustable small holes, and the bottom of the dark room is equipped with an electric shock device. If mice escape from the dark room to the dark room, they will be shocked immediately. The experiment was divided into two days of Training and Test at an interval of 24 h.

Training: close the hole between the bright room and the hint before starting, open the boot cover and p, At first, lace the mouse in the bright room for 5 min to adapt to the environment. Then turn on the power (the sustained electric shock starts from the bottom of the dark chamber), open the hole at the same time, observe and record the latency of the corresponding mice, which is the time when the mice enter the dark chamber from the open chamber for the first time. The Number of errors was the Number of times that the mice entered the dark room from the open room. The incubation period and Error times of the mice within 300s were observed and recorded.

Test: clean the experimental equipment and remove the smell to ensure that the environment is basically consistent with the training. Test was performed on the 24th h after the training of mice, the hole was closed before startup, the hole was opened immediately after the mice were put into the open chamber and the electric power was switched on. Latency and error times of the corresponding mice were observed and recorded.

Statistical Analysis

Data are presented as mean ± SEM. The data are from at least three different experiments, with each data point within an individual experiment representing triplicate measurements. Statistical analyses were performed using SPSS 13.0. Values were compared using the Nonparametric Kruskal – Wallis One-way ANOVA followed by the Dunn post hoc test was used to determine the statistical significance

between multiple groups and the Wilcoxon test was used to compare between 2 groups .The results were considered statistically significant when $P < 0.05$.

Abbreviations

ACSF : Artificial cerebro-Spinal Fluid; cART : Combined antiretroviral therapy; AIDS: Acquired immune deficiency syndrome; CNS: Central nervous system; HAND: HIV-1 associated neurocognitive disorder; Iba1: ionized calcium binding adapter molecule 1; IL-1β: Interleukin 1 Beta; iNOS: inducible nitric oxide synthase; Keap-1: Kelch-like ECH-associated protein 1; MCP-1: mono-cyte chemotactic protein-1; NO: Nitric oxide; Nrf2: nuclear factor erythroid related factor 2; RAPA: rapamycin; RNAi: RNA interference; siRNA: Small interfering RNA; TNF-α: tumor necrosis factor-α; 3-MA: 3-Methyladenine.

Declarations

Funding

This work was supported by grants from the National Natural Science Foundation of China (81974185), Guangdong Provincial Natural Science Foundation of China (2014A030313360 and 2019A1515012024), the Program of Introducing Talents of Discipline to Universities (B14036), the Science and Technology Foundation of Guangdong (2010B030700016), the cultivation and innovation fund of Jinan University (No.21617460), and the medical group fund of Jinan University (88016013039).

Competing interests

The authors declare that they have no conflicts of interest.

Availability of data and material

The data sets supporting the results of this article are included within the article and its additional files.

Authors' contributions

JD (Jun Dong) designed the study. SL (Sisi Liu) performed the studies, XY (Xueqin Yan) and HH (Hanyang He) assisted in part of the experiment. RP (Rui Pan), HW (Huili Wang) and HT (HaijieTang) analysed the data and interpreted the results. SL and JD wrote the paper. XY and HH help edit the paper. All authors read and approved the final manuscript.

Ethics approval and consent to participate

No human data or tissues were used in this study. All animal experimental protocols and handling procedures were approved by the Laboratory Animal Ethics Committee of Jinan University.

Consent for publication

Not applicable.

References

1. Navia BA, Jordan BD, Price RW (1986) The AIDS dementia complex: I. Clinical features. Ann Neurol 19(6):517–524. doi:10.1002/ana.410190602
2. McArthur JC, Hoover DR, Bacellar H, Miller EN, Cohen BA, Becker JT, Graham NM, McArthur JH, Selnes OA, Jacobson LP et al (1993) Dementia in AIDS patients: incidence and risk factors. Multicenter AIDS Cohort Study. Neurology 43(11):2245–2252
3. McArthur JC, Steiner J, Sacktor N, Nath A (2010) Human immunodeficiency virus-associated neurocognitive disorders: Mind the gap. Ann Neurol 67(6):699–714. doi:10.1002/ana.22053
4. Heaton RK, Franklin DR, Ellis RJ, McCutchan JA, Letendre SL, Leblanc S, Corkran SH, Duarte NA, Clifford DB, Woods SP, Collier AC, Marra CM, Morgello S, Mindt MR, Taylor MJ, Marcotte TD, Atkinson JH, Wolfson T, Gelman BB, McArthur JC, Simpson DM, Abramson I, Gamst A, Fennema-Notestine C, Jernigan TL, Wong J, Grant I, Group C, Group H (2011) HIV-associated neurocognitive disorders before and during the era of combination antiretroviral therapy: differences in rates, nature, and predictors. J Neurovirol 17(1):3–16. doi:10.1007/s13365-010-0006-1
5. Sacktor N, Skolasky RL, Seaberg E, Munro C, Becker JT, Martin E, Ragin A, Levine A, Miller E (2016) Prevalence of HIV-associated neurocognitive disorders in the Multicenter AIDS Cohort Study. Neurology 86(4):334–340. doi:10.1212/WNL.0000000000002277
6. Eggers C, Arendt G, Hahn K, Husstedt IW, Maschke M, Neuen-Jacob E, Obermann M, Rosenkranz T, Schielke E, Straube E, German Association of Neuro AuN-I (2017) HIV-1-associated neurocognitive disorder: epidemiology, pathogenesis, diagnosis, and treatment. J Neurol 264(8):1715–1727. doi:10.1007/s00415-017-8503-2
7. Shaw GM, Harper ME, Hahn BH, Epstein LG, Gajdusek DC, Price RW, Navia BA, Petito CK, O'Hara CJ, Groopman JE et al (1985) HTLV-III infection in brains of children and adults with AIDS encephalopathy. Science 227(4683):177–182
8. Chen G, Liu S, Pan R, Li G, Tang H, Jiang M, Xing Y, Jin F, Lin L, Dong J (2018) Curcumin Attenuates gp120-Induced Microglial Inflammation by Inhibiting Autophagy via the PI3K Pathway. Cell Mol Neurobiol 38(8):1465–1477. doi:10.1007/s10571-018-0616-3
9. Katsuragi Y, Ichimura Y, Komatsu M (2015) p62/SQSTM1 functions as a signaling hub and an autophagy adaptor. FEBS J 282(24):4672–4678. doi:10.1111/febs.13540
10. Jiang T, Harder B, Rojo de la Vega M, Wong PK, Chapman E, Zhang DD (2015) p62 links autophagy and Nrf2 signaling. Free Radic Biol Med 88(Pt B):199–204. doi:10.1016/j.freeradbiomed.2015.06.014
11. von Haefen C, Sifringer M, Endesfelder S, Kalb A, Gonzalez-Lopez A, Tegethoff A, Paeschke N, Spies CD (2018) Physostigmine Restores Impaired Autophagy in the Rat Hippocampus after Surgery Stress and LPS Treatment. J Neuroimmune Pharmacol 13(3):383–395. doi:10.1007/s11481-018-9790-9

12. Jin GL, Yue RC, He SD, Hong LM, Xu Y, Yu CX (2018) Koumine Decreases Astrocyte-Mediated Neuroinflammation and Enhances Autophagy, Contributing to Neuropathic Pain From Chronic Constriction Injury in Rats. Front Pharmacol 9:989. doi:10.3389/fphar.2018.00989
13. Du D, Hu L, Wu J, Wu Q, Cheng W, Guo Y, Guan R, Wang Y, Chen X, Yan X, Zhu D, Wang J, Zhang S, Guo Y, Xia C (2017) Neuroinflammation contributes to autophagy flux blockage in the neurons of rostral ventrolateral medulla in stress-induced hypertension rats. J Neuroinflammation 14(1):169. doi:10.1186/s12974-017-0942-2
14. Motohashi H, Yamamoto M (2004) Nrf2-Keap1 defines a physiologically important stress response mechanism. Trends Mol Med 10(11):549–557. doi:10.1016/j.molmed.2004.09.003
15. Lau A, Wang XJ, Zhao F, Villeneuve NF, Wu T, Jiang T, Sun Z, White E, Zhang DD (2010) A noncanonical mechanism of Nrf2 activation by autophagy deficiency: direct interaction between Keap1 and p62. Mol Cell Biol 30(13):3275–3285. doi:10.1128/MCB.00248-10
16. Jain A, Lamark T, Sjottem E, Larsen KB, Awuh JA, Overvatn A, McMahon M, Hayes JD, Johansen T (2010) p62/SQSTM1 Is a Target Gene for Transcription Factor NRF2 and Creates a Positive Feedback Loop by Inducing Antioxidant Response Element-driven Gene Transcription. J Biol Chem 285(29):22576–22591. doi:10.1074/jbc.M110.118976
17. Pajares M, Jimenez-Moreno N, Garcia-Yague AJ, Escoll M, de Ceballos ML, Van Leuven F, Rabano A, Yamamoto M, Rojo AI, Cuadrado A (2016) Transcription factor NFE2L2/NRF2 is a regulator of macroautophagy genes. Autophagy 12(10):1902–1916. doi:10.1080/15548627.2016.1208889
18. Rock RB, Gekker G, Hu S, Sheng WS, Cheeran M, Lokensgard JR, Peterson PK (2004) Role of microglia in central nervous system infections. Clin Microbiol Rev 17(4):942–964. doi:10.1128/CMR.17.4.942-964.2004 table of contents.
19. Garvey LJ, Pavese N, Politis M, Ramlackhansingh A, Brooks DJ, Taylor-Robinson SD, Winston A (2014) Increased microglia activation in neurologically asymptomatic HIV-infected patients receiving effective ART. AIDS 28(1):67–72. doi:10.1097/01.aids.0000432467.54003.f7
20. Sieweke MH, Allen JE (2013) Beyond stem cells: self-renewal of differentiated macrophages. Science 342(6161):1242974. doi:10.1126/science.1242974
21. Huang CC, Tang M, Zhang MY, Majeed S, Montabana E, Stanfield RL, Dimitrov DS, Korber B, Sodroski J, Wilson IA, Wyatt R, Kwong PD (2005) Structure of a V3-containing HIV-1 gp120 core. Science 310(5750):1025–1028. doi:10.1126/science.1118398
22. Zolla-Pazner S (2005) Improving on nature: focusing the immune response on the V3 loop. Hum Antibodies 14(3–4):69–72
23. Alirezaei M, Kiosses WB, Fox HS (2008) Decreased neuronal autophagy in HIV dementia - A mechanism of indirect neurotoxicity. Autophagy 4(7):963–966. doi:DOI 10.4161/auto.6805
24. El-Hage N, Rodriguez M, Dever SM, Masvekar RR, Gewirtz DA, Shacka JJ (2015) HIV-1 and morphine regulation of autophagy in microglia: limited interactions in the context of HIV-1 infection and opioid abuse. J Virol 89(2):1024–1035. doi:10.1128/JVI.02022-14

25. Liu S, Xing Y, Wang J, Pan R, Li G, Tang H, Chen G, Yan L, Guo L, Jiang M, Gong Z, Lin L, Dong J (2019) The Dual Role of HIV-1 gp120 V3 Loop-Induced Autophagy in the Survival and Apoptosis of the Primary Rat Hippocampal Neurons. Neurochem Res 44(7):1636–1652. doi:10.1007/s11064-019-02788-3
26. Pankiv S, Clausen TH, Lamark T, Brech A, Bruun JA, Outzen H, Overvatn A, Bjorkoy G, Johansen T (2007) p62/SQSTM1 binds directly to Atg8/LC3 to facilitate degradation of ubiquitinated protein aggregates by autophagy. J Biol Chem 282(33):24131–24145. doi:10.1074/jbc.M702824200
27. Rodriguez A, Duran A, Selloum M, Champy MF, Diez-Guerra FJ, Flores JM, Serrano M, Auwerx J, Diaz-Meco MT, Moscat J (2006) Mature-onset obesity and insulin resistance in mice deficient in the signaling adapter p62. Cell Metab 3(3):211–222. doi:10.1016/j.cmet.2006.01.011
28. Moscat J, Diaz-Meco MT (2011) Feedback on fat: p62-mTORC1-autophagy connections. Cell 147(4):724–727. doi:10.1016/j.cell.2011.10.021
29. Yu SZ, Wang Y, Jing L, Claret FX, Li Q, Tian T, Liang X, Ruan ZP, Jiang LL, Yao Y, Nan KJ, Lv Y, Guo H (2017) Autophagy in the "inflammation-carcinogenesis" pathway of liver and HCC immunotherapy. Cancer Lett 411:82–89. doi:10.1016/j.canlet.2017.09.049
30. Fabrizi C, Pompili E, Somma F, De Vito S, Ciraci V, Artico M, Lenzi P, Fornai F, Fumagalli L (2017) Lithium limits trimethyltin-induced cytotoxicity and proinflammatory response in microglia without affecting the concurrent autophagy impairment. J Appl Toxicol 37(2):207–213. doi:10.1002/jat.3344
31. Tanji K, Maruyama A, Odagiri S, Mori F, Itoh K, Kakita A, Takahashi H, Wakabayashi K (2013) Keap1 is localized in neuronal and glial cytoplasmic inclusions in various neurodegenerative diseases. J Neuropathol Exp Neurol 72(1):18–28. doi:10.1097/NEN.0b013e31827b5713
32. Tanji K, Miki Y, Ozaki T, Maruyama A, Yoshida H, Mimura J, Matsumiya T, Mori F, Imaizumi T, Itoh K, Kakita A, Takahashi H, Wakabayashi K (2014) Phosphorylation of serine 349 of p62 in Alzheimer's disease brain. Acta Neuropathol Commun 2:50. doi:10.1186/2051-5960-2-50
33. Yamazaki H, Tanji K, Wakabayashi K, Matsuura S, Itoh K (2015) Role of the Keap1/Nrf2 pathway in neurodegenerative diseases. Pathol Int 65(5):210–219. doi:10.1111/pin.12261
34. Jain A, Lamark T, Sjottem E, Larsen KB, Awuh JA, Overvatn A, McMahon M, Hayes JD, Johansen T (2010) p62/SQSTM1 is a target gene for transcription factor NRF2 and creates a positive feedback loop by inducing antioxidant response element-driven gene transcription. J Biol Chem 285(29):22576–22591. doi:10.1074/jbc.M110.118976
35. Taguchi K, Fujikawa N, Komatsu M, Ishii T, Unno M, Akaike T, Motohashi H, Yamamoto M (2012) Keap1 degradation by autophagy for the maintenance of redox homeostasis. P Natl Acad Sci USA 109(34):13561–13566. doi:10.1073/pnas.1121572109
36. Zhang X, Bedard EL, Potter R, Zhong R, Alam J, Choi AM, Lee PJ (2002) Mitogen-activated protein kinases regulate HO-1 gene transcription after ischemia-reperfusion lung injury. Am J Physiol Lung Cell Mol Physiol 283(4):L815–L829. doi:10.1152/ajplung.00485.2001
37. Tang H, Lu D, Pan R, Qin X, Xiong H, Dong J (2009) Curcumin improves spatial memory impairment induced by human immunodeficiency virus type 1 glycoprotein 120 V3 loop peptide in rats. Life Sci

85(1–2):1–10. doi:10.1016/j.lfs.2009.03.013

38. Olayanju A, Copple IM, Bryan HK, Edge GT, Sison RL, Wong MW, Lai ZQ, Lin ZX, Dunn K, Sanderson CM, Alghanem AF, Cross MJ, Ellis EC, Ingelman-Sundberg M, Malik HZ, Kitteringham NR, Goldring CE, Park BK (2015) Brusatol provokes a rapid and transient inhibition of Nrf2 signaling and sensitizes mammalian cells to chemical toxicity-implications for therapeutic targeting of Nrf2. Free Radic Biol Med 78:202–212. doi:10.1016/j.freeradbiomed.2014.11.003
39. Turpaev K, Welsh N (2015) Brusatol inhibits the response of cultured beta-cells to pro-inflammatory cytokines in vitro. Biochem Biophys Res Commun 460(3):868–872. doi:10.1016/j.bbrc.2015.03.124
40. Oh ET, Kim CW, Kim HG, Lee JS, Park HJ (2017) Brusatol-Mediated Inhibition of c-Myc Increases HIF-1alpha Degradation and Causes Cell Death in Colorectal Cancer under Hypoxia. Theranostics 7(14):3415–3431. doi:10.7150/thno.20861
41. Morris RG, Garrud P, Rawlins JN, O'Keefe J (1982) Place navigation impaired in rats with hippocampal lesions. Nature 297(5868):681–683

Figures

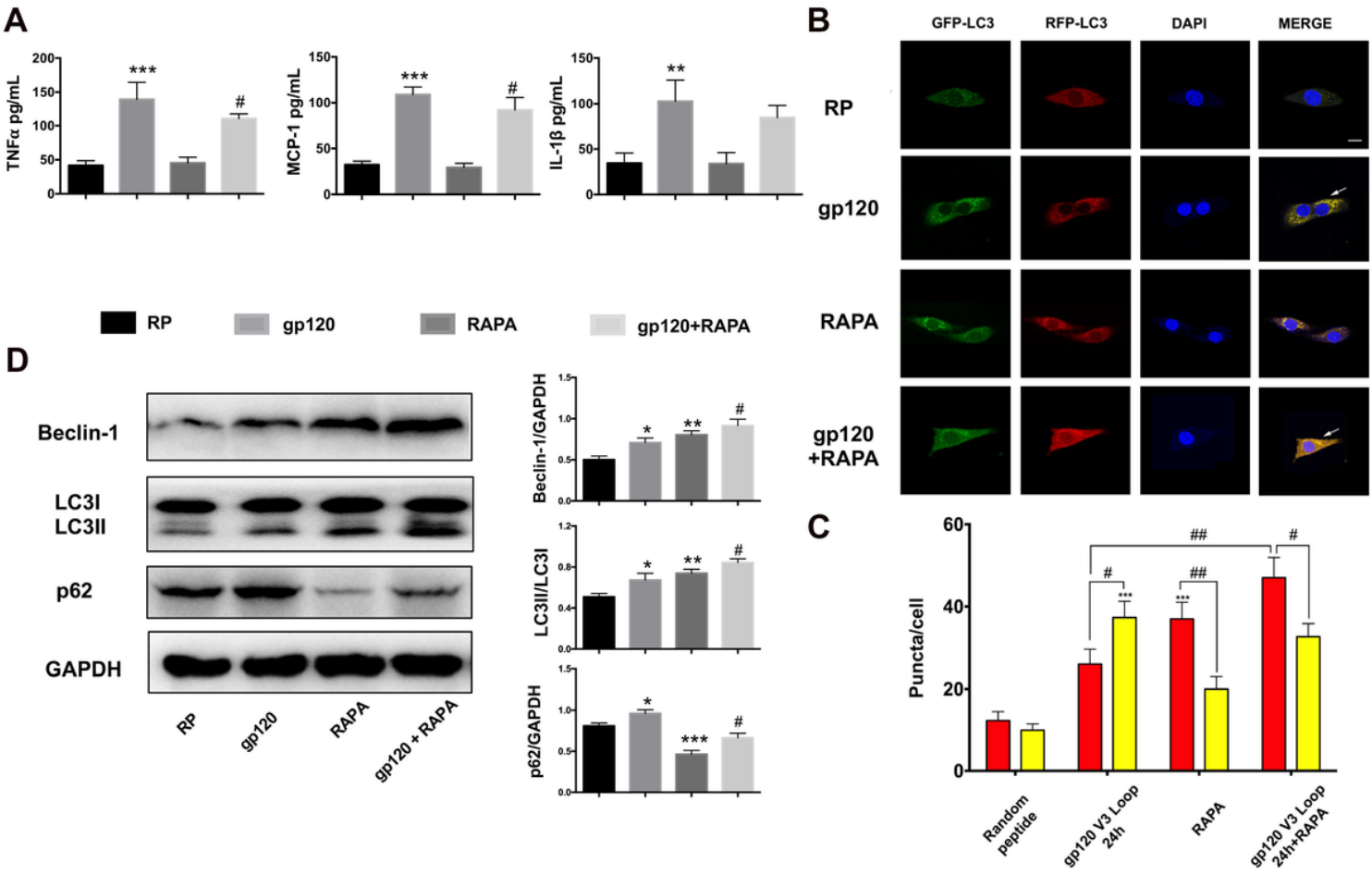

Figure 1

HIV-1 gp120 V3 loop leads to autophagy dysfunction and promotes inflammation in CHME-5 cells. (A) Concentrations of TNF-α, MCP-1 and IL-1β form each group detected by ELISA. (B) CHME-5 cells transfected with GFP-RFP-LC3 adenovirus followed by HIV-1 gp120 V3 loop (1 μg/mL) and treated with rapamycin (20 nM) for 24 h. Scale bar: 10 μm. (C) Bar graph showing the number of autophagosomes (yellow) and autolysosomes (red) in (B). (D) Representative western blots showing the expression of Beclin-1, LC3-II and p62 in CHME-5 cells. The presented as mean ± SEM from 6 independent experiments. Nonparametric Kruskal – Wallis One-way ANOVA followed by the Dunn post hoc test was used to determine the statistical significance between multiple groups and the Wilcoxon test was used to compare between 2 groups: *p < 0.05, **p< 0.01 and ***p< 0.001 vs. control, #p < 0.05, ##p< 0.01 vs. gp120 V3 loop.

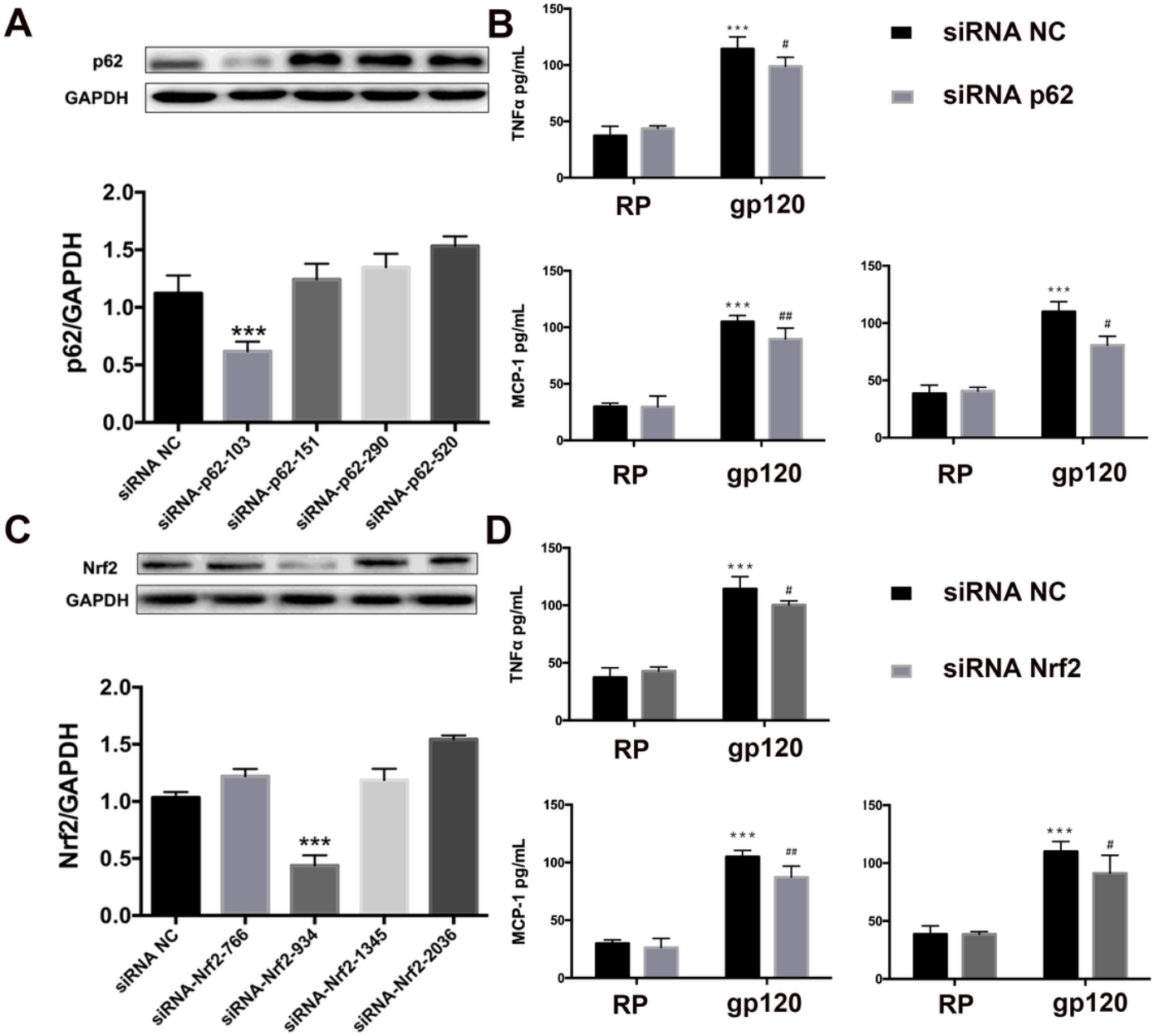

Figure 2

Gene silencing of p62 and Nrf2 inhibited HIV-1 gp120 V3 loop mediated inflammation in CHME-5 cells. (A) Representative western blots showing the expression of p62 in CHME-5 cells transfected with either p62 siRNA or scrambled siRNA (B) concentrations of TNF-α, MCP-1 and IL-1β form cell supernatant detected by ELISA in CHME-5 cells transfected with p62 siRNA and scrambled siRNA, (C) Representative western blots showing the expression of p62 in CHME-5 cells transfected with either Nrf2 siRNA or scrambled siRNA, (D) concentrations of TNF-α, MCP-1 and IL-1β form cell supernatant detected by ELISA in CHME-5 cells transfected with Nrf2 siRNA and scrambled siRNA, The data are presented as mean ± SEM from 6 independent experiments. Nonparametric Kruskal-Wallis One-way ANOVA followed by the Dunn post hoc test was used to determine the statistical significance between multiple groups. ***p< 0.001 vs. control, #p < 0.05, ##p< 0.01 vs. gp120 V3 loop.

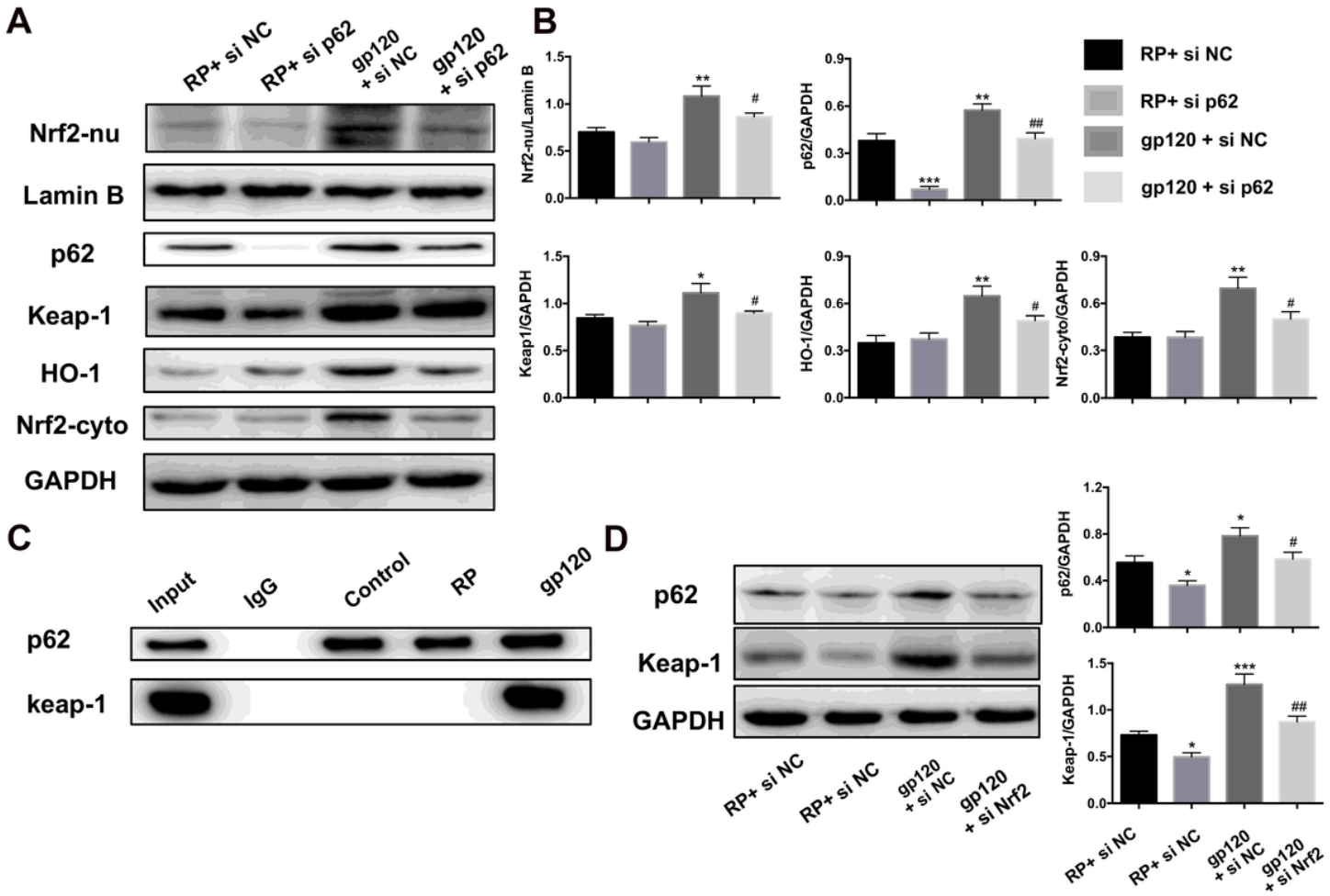

Figure 3

Nrf2 noncanonical activated in HIV-1 gp120 V3 loop treated CHME-5 cells. (A) Representative immunoblots and (B) quantification expressions of the indicated protein in CHME-5 cells transfected with either p62 siRNA or scrambled siRNA following exposure to HIV-1 gp120 V3 loop for 24 h. (C) Whole cell lysates were immunoprecipitated (IP) with anti–p62 antibody and then analyzed by immunoblotting (IB) using anti–Keap-1 antibody.(D) Representative immunoblots of p62 and keap-1and quantification expressions of the indicated protein in CHME-5 cells transfected with either Nrf2 siRNA or scrambled

siRNA following exposure to HIV-1 gp120 V3 loop for 24 h. Nonparametric Kruskal-Wallis One-way ANOVA followed by the Dunn post hoc test was used to determine the statistical significance between multiple groups. *p < 0.05, **p< 0.01 and ***p< 0.001 vs. control, #p < 0.05, ##p< 0.01 vs. gp120 V3 loop.

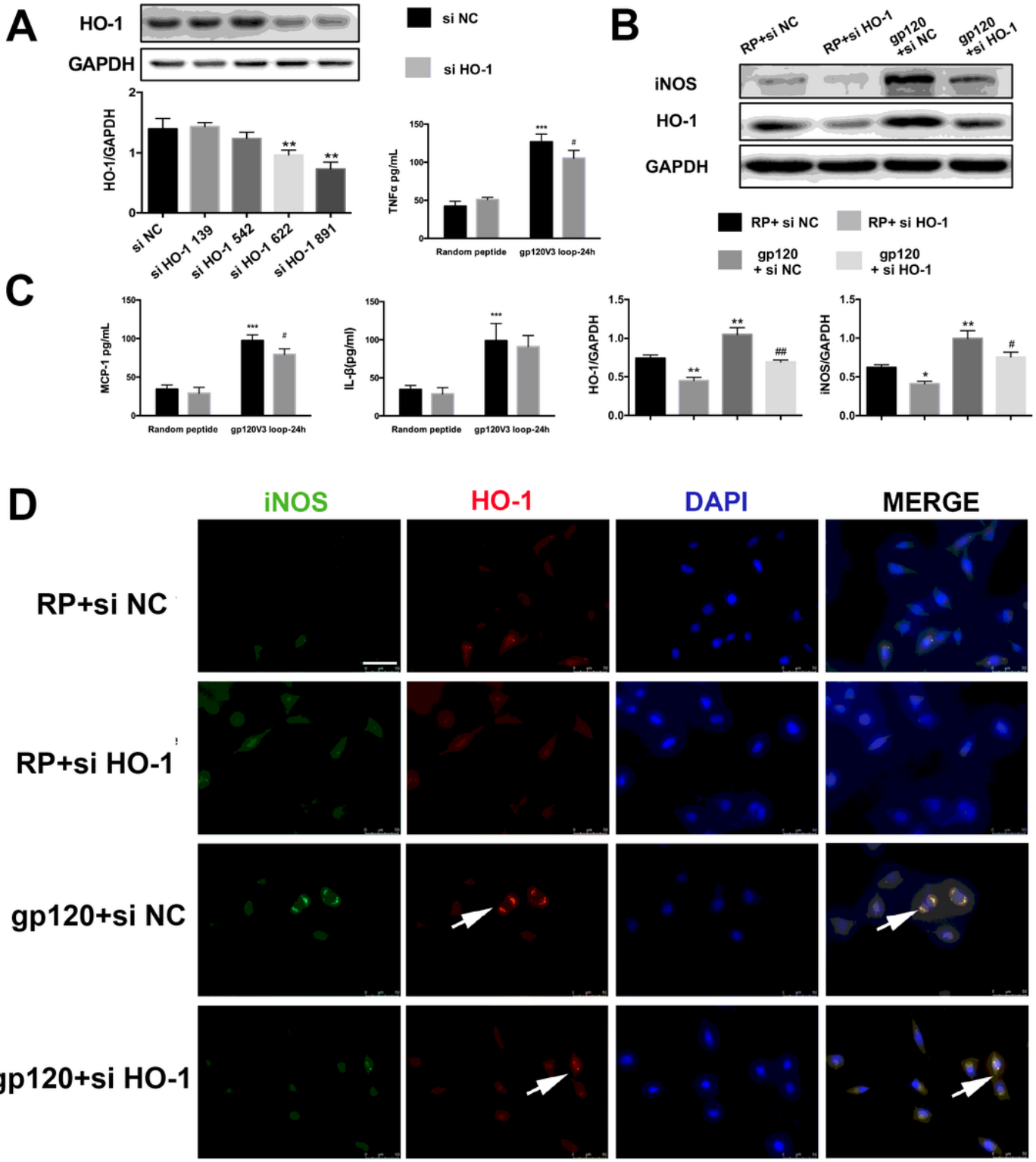

Figure 4

HO-1 promotes iNOS expression by interacting with iNOS to promote inflammation in HIV-1 gp120 V3 loop treated CHME-5 cells. (A) Representative immunoblots and quantification expressions of the

indicated protein in CHME-5 cells transfected with either HO-1siRNA or scrambled siRNA, (B) Representative immunoblots and quantification expressions of the indicated protein in CHME-5 cells transfected with either HO-1 siRNA and scrambled siRNA following exposure to HIV-1 gp120 V3 loop for 24 h. (C) concentrations of TNF-α, MCP-1 and IL-1β form cell supernatant detected by ELISA in CHME-5 cells transfected with HO-1 siRNA or scrambled siRNA, (D) Fluorescence microscope detection of iNOS (green) and HO-1 (red) in CHME-5 cells. Yellow indicates colocalization of iNOS and LC3 (white arrow). CHME-5 cells transfected with either HO-1 siRNA or scrambled siRNA following exposure to HIV-1 gp120 V3 loop for 24 h. The data are presented as mean ± SEM from 6 independent experiments. Nonparametric Kruskal-Wallis One-way ANOVA followed by the Dunn post hoc test was used to determine the statistical significance between multiple groups. *p < 0.05, **p< 0.01 and ***p< 0.001 vs. control, #p < 0.05, ##p< 0.01 vs. gp120 V3 loop.

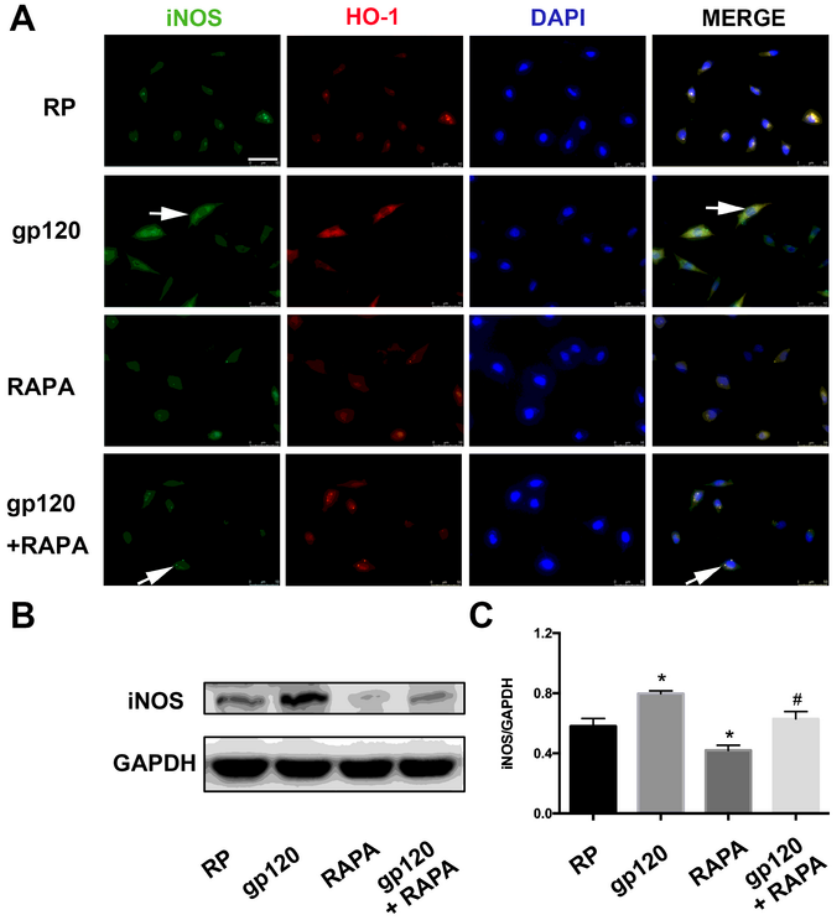

Figure 5

HO-1 promotes iNOS expression by interacting with iNOS to promote inflammation in HIV-1 gp120 V3 loop treated CHME-5 cells. (A) Representative immunoblots and quantification expressions of the indicated protein in CHME-5 cells transfected with either HO-1siRNA or scrambled siRNA, (B) Representative immunoblots and quantification expressions of the indicated protein in CHME-5 cells transfected with either HO-1 siRNA and scrambled siRNA following exposure to HIV-1 gp120 V3 loop for 24 h. (C) concentrations of TNF-α, MCP-1 and IL-1β form cell supernatant detected by ELISA in CHME-5

cells transfected with HO-1 siRNA or scrambled siRNA, (D) Fluorescence microscope detection of iNOS (green) and HO-1 (red) in CHME-5 cells. Yellow indicates colocalization of iNOS and LC3 (white arrow). CHME-5 cells transfected with either HO-1 siRNA or scrambled siRNA following exposure to HIV-1 gp120 V3 loop for 24 h. The data are presented as mean ± SEM from 6 independent experiments. Nonparametric Kruskal-Wallis One-way ANOVA followed by the Dunn post hoc test was used to determine the statistical significance between multiple groups. *p < 0.05, **p< 0.01 and ***p< 0.001 vs. control, #p < 0.05, ##p< 0.01 vs. gp120 V3 loop.

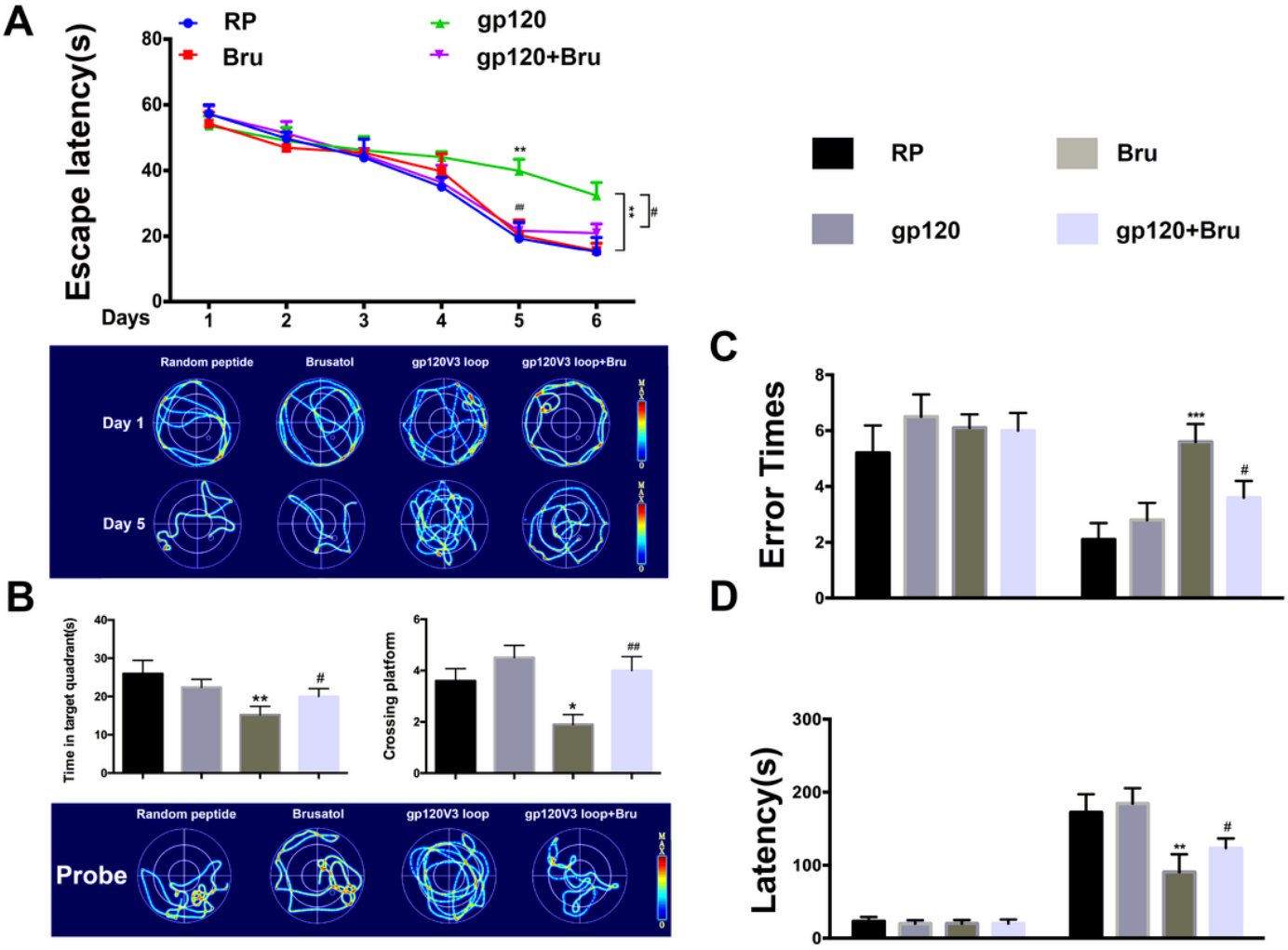

Figure 6

Brusatol alleviated neurocognitive dysfunction in mice induced by HIV-1 gp120 V3 loop. (A) The latency of each group of mice in the place navigation test of Morris water maze test and representative tracks of each group at day 1th and 5th. (B) time in the target quadrant and crossing platform number of each group in the spatial probe test, and representative tracks of each group in the spatial probe test of Morris water maze test. (C) Error times and (d) latency of mice in each group tested by Step-through passive avoidance test(n=10). Nonparametric Kruskal-Wallis One-way ANOVA followed by the Dunn post hoc test was used to determine the statistical significance between multiple groups. *p < 0.05, **p< 0.01 and ***p< 0.001 vs. control, #p < 0.05, ##p< 0.01 vs. gp120 V3 loop.

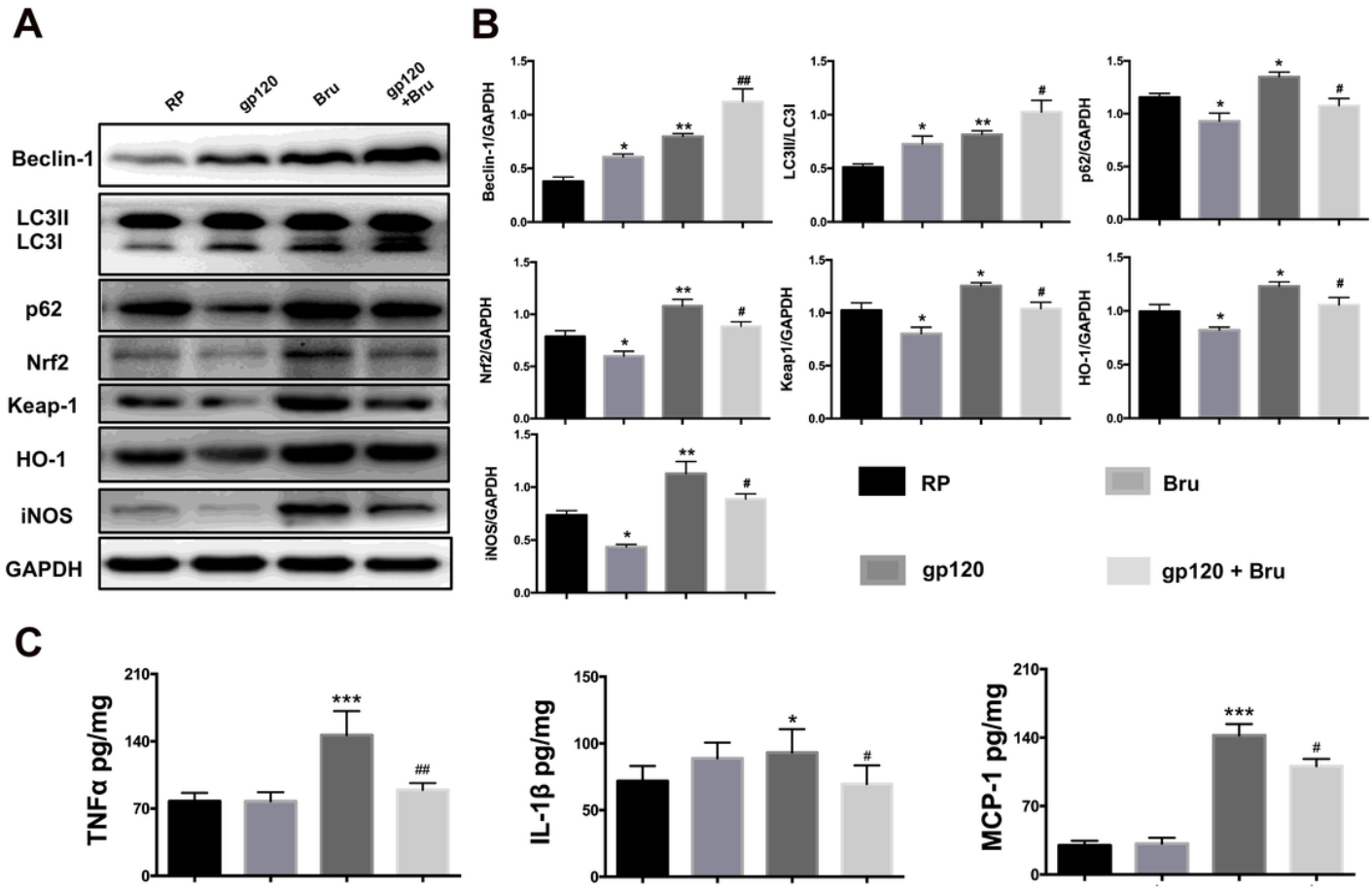

Figure 7

Brusatol inhibited HIV-1 gp120 V3 loop mediated increased autophagy markers expression, and proinflammatory cytokines in vivo. (A) Representative immunoblots and (B) quantification expressions of Beclin-1, LC3, p62, Nrf2, Keap-1, HO-1 and iNOS, (C) Levels of TNF-α, IL-1β, and MCP-1 in the mice brain tissue form each group were measured by ELISA. The data are presented as mean ± SEM from 6 independent experiments. Kruskal-Wallis One-way ANOVA followed by the Dunn post hoc test was used to determine the statistical significance between multiple groups. *p < 0.05, **p< 0.01 and ***p< 0.001 vs. control, #p < 0.05, ##p< 0.01 vs. gp120 V3 loop.

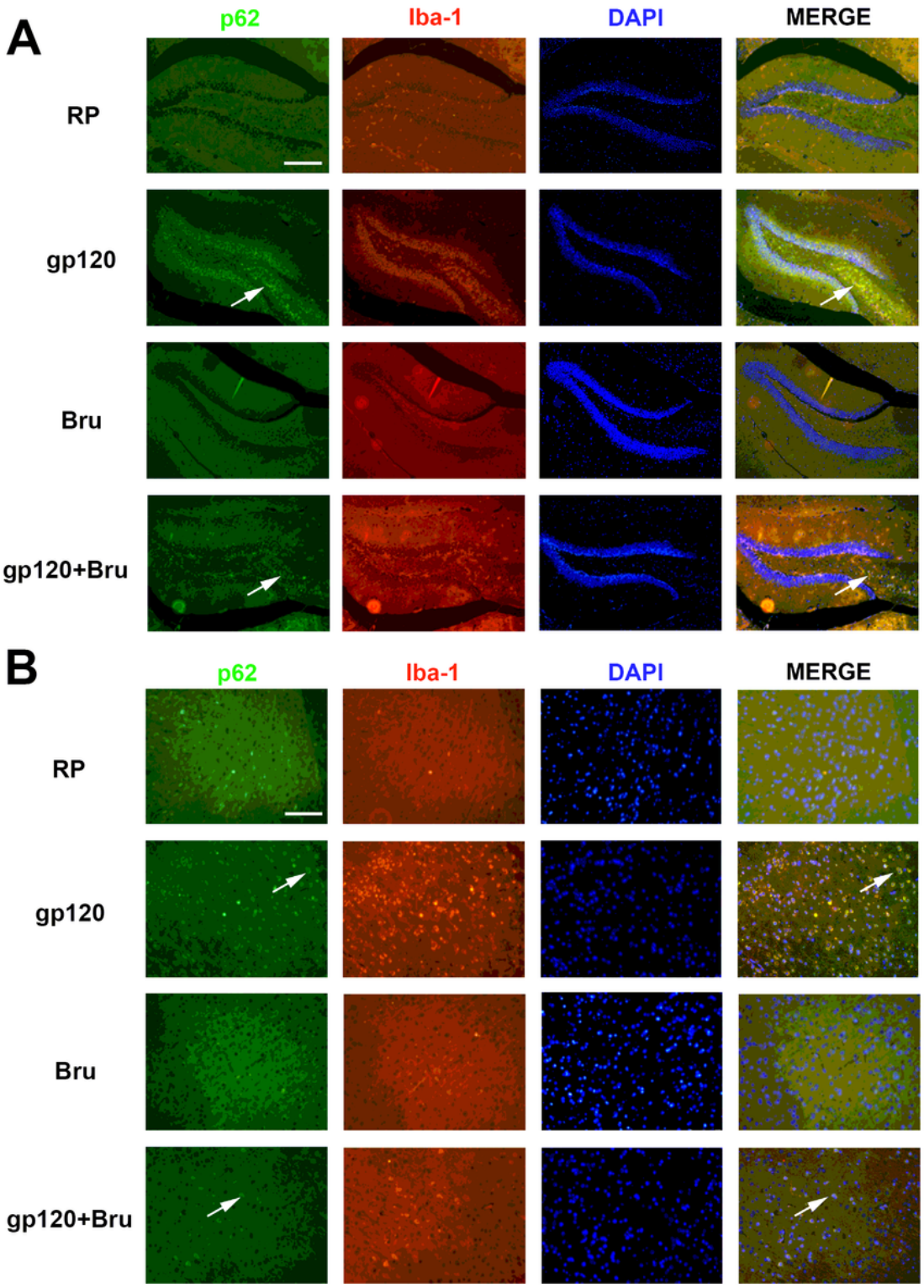

Figure 8

HIV-1 gp120 V3 loop mediated upregulation of p62 and microglial activation in vivo.Immunofluorescence staining for p62 (green), Iba-1, microglial marker (red), and DAPI (blue) in (A) the hippocampus and (B) the frontal cortices of mice treated with HIV-1 gp120 V3 loop or Brusatol . Scale bar: (A) 250 μm and (B) 100 μm.